Electronic theory of Bloch walls in ferromagnets

J. Schwitalla and B. L. Györffy
H. H. Wills Physics Laboratory, University of Bristol, Tyndall Avenue, Bristol BS8-1TL, United Kingdom

L. Szunyogh
Department of Theoretical Physics, Budapest University of Technology and Economics, Budafoki út 8, 1521 Budapest, Hungary and Center for Computational Materials Science, Technical University of Vienna, Gumpendorferstr. 1A, A-1060 Vienna, Austria

(Received 5 July 2000; published 20 February 2001)

Bloch walls are treated on the basis of the relativistic spin-density functional theory in the local density approximation. We implement the proposed theory and determine the Bloch wall thickness in bcc Fe. Moreover, we study the features of the electronic structure, such as the variations of the density of states and of the magnetic moments, which arise due to the presence of the Bloch wall.

DOI: 10.1103/PhysRevB.63.104423 PACS number(s): 75.60.Ch, 75.30.Gw, 71.15.Ap

I. INTRODUCTION

Domains of different magnetic orientations spontaneously nucleate in all magnetic materials in order to minimize the magnetostatic energy (dipolar interaction) of the system. These domains are separated by domain or Bloch walls where the magnetization is changing over, rapidly, from one orientation to an other. In this paper we shall develop a theoretical account of these transition regions in terms of mobile electrons and their spins, that is to say from first principles.

The understanding and control of the domain structure, magnetic morphology, is central to the effective use of magnetic materials in many technologies.[1] Moreover, the nature, shape, and motion of Bloch walls have always attracted fundamental scientific interest.[2–8] Nevertheless, all the theoretical discussions so far, of the entire subject, have been strictly phenomenological. In the present paper we wish to lay the foundation of a first-principles approach to the problem.

To start with a tractable problem, henceforth, we shall focus on that of a single Bloch wall. Note that while its width, $l_{BW}\sim 10-1000$ nm, is much larger than the lattice spacing a, it is the smallest of all the other length scales such as the sizes of the domains, $1-1000$ μm, and the magnetic texture, >0.1 mm, etc. in the problem. Thus, by deploying our first-principles methodology, designed to treat variations in properties on the length-scale a, to Bloch wall problems, we are making the natural choice of crossing the smallest scale gap first.

The established theory of Bloch walls is a topic in micromagnetics[7] and it is wholly phenomenological. It consists of the equations of Landau and Lifshitz[4] as generalized by Brown.[8] For clarity and easy future reference, we summarize here the part of this theoretical framework relevant to our present concern. In short, the magnetization density is described by the vector field $\vec{M}(\vec{r},t)$, which evolves in time according to the Landau-Lifshitz equation,

$$\frac{\partial \vec{M}}{\partial t}=\frac{2\mu_{\mathrm{B}}}{\hbar}\vec{M}\times\frac{\delta \mathcal{F}[\vec{M}]}{\delta \vec{M}}, \tag{1}$$

where μ_{B} is the Bohr magneton, $\hbar$ is the Planck constant and $\mathcal{F}[\vec{M}]$ is a generalized free-energy functional of $\vec{M}(\vec{r},t)$. For our present purposes it will be sufficient to take the $\mathcal{F}[\vec{M}]$ to be given by the usual Ginzburg-Landau expansion,

$$\mathcal{F}[\vec{M}]\approx\int d\vec{r}\Bigg\{\mathcal{A}\sum_{i=1}^{3}|\vec{\nabla}M_i|^2+\sum_{i,j=1}^{3}\mathcal{B}_{ij}M_iM_j+\sum_{i,j,k,l=1}^{3}\mathcal{B}_{ijkl}M_iM_jM_kM_l+\ldots\Bigg\}, \tag{2}$$

where i and j refer to Cartesian axes x,y, and z, and the coefficients $\mathcal{A}$, $\mathcal{B}_{ij}$, and $\mathcal{B}_{ijkl}$ are material specific parameters which depend on such thermodynamic variables as temperature, T, and pressure, p. Evidently, the equilibrium magnetization, $\vec{M}_{eq}$, which minimizes $\mathcal{F}[\vec{M}]$ is a stationary solution of Eq. (1). The simplest Bloch wall like solution of these equations follow from parametrizing the Cartesian components M_i in terms of spherical coordinates θ and ϕ (see Fig. 1)

$$M_{\mathrm{x}}=M_0\cos\phi\sin\theta,\quad M_{\mathrm{y}}=M_0\sin\phi\sin\theta,\quad M_{\mathrm{z}}=M_0\cos\theta, \tag{3}$$

where M_0 is a constant equal to the saturation magnetization, and stopping the expansion in Eq. (2) at the 4th order. For a cubic system $[\mathcal{B}_{ij}=0$ and $\mathcal{B}_{ijkl}=\delta_{ij}\delta_{kl}(\mathcal{B}_1(1-\delta_{ik})+\mathcal{B}_2\delta_{ik})]$ this means

$$\mathcal{F}(\theta,\phi)=\int\{\alpha[(\vec{\nabla}\theta(\vec{r}))^2+\sin^2\theta(\vec{r})(\vec{\nabla}\phi(\vec{r}))^2]+\beta[\sin^2\theta(\vec{r})\cos^2\theta(\vec{r})+\sin^4\theta(\vec{r})\sin^2\phi(\vec{r})\cos^2\phi(\vec{r})]\}d\vec{r}, \tag{4}$$

where the coefficients are defined as $\alpha=\mathcal{A}M_0^2$ and $\beta=2(\mathcal{B}_1-\mathcal{B}_2)M_0^4$, respectively, and a trivial constant term has been dropped. Taking $\theta=\pi/2$ and ϕ a function of the z coordinate only, Eq. (4) reduces to

$$\mathcal{F}(\phi)=\int\{\alpha[\vec{\nabla}\phi(\vec{r})]^2+\beta\sin^2\phi(\vec{r})\cos^2\phi(\vec{r})\}d\vec{r}. \tag{5}$$

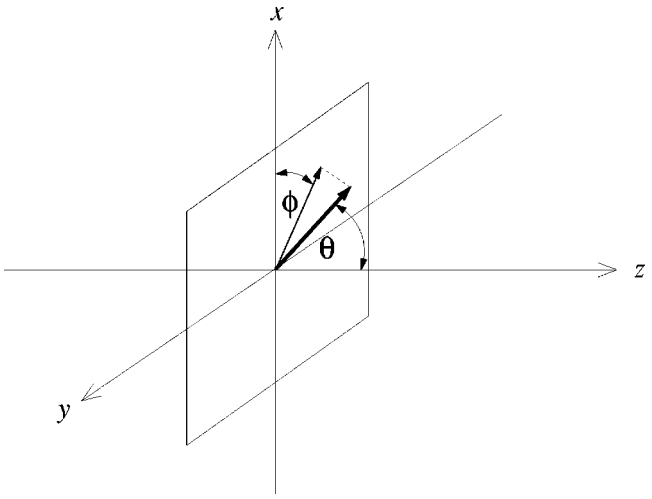

FIG. 1. Sketch of the spherical coordinates, θ and ϕ, as used throughout in the paper.

It can be readily shown[9] that, subject to the boundary conditions $\phi(-\infty)=0$ and $\phi(\infty)=\pi/2$, the function

$$\phi(z)=\arctan \mathrm{e}^{\sqrt{\frac{\beta}{\alpha}}z} \tag{6}$$

minimizes $\mathcal{F}(\phi)$ in Eq. (5). In what follows we shall study this simple example of a 90° Bloch wall from the point of view of mobile electron whose spin gives rise to such magnetic configuration.

Given the success and the general satisfaction with the established phenomenological theory outlined above one may, at this stage, protest that such microscopic considerations are not needed. To answer this objection we shall now pause briefly to argue the case to the contrary. In the interest of economy we present our arguments as a list of brief statements:

(a) Firstly, the phenomenological theory assumes that $\vec{M}(z)$ rotates as z goes from $-\infty$ to ∞ without a change in magnitude. A first-principles theory should tell us if and when this is true.

(b) Because, as yet, experiments cannot tell us otherwise,[10] the phenomenological theory accepts the form of $\phi(z)$ in Eq. (6) as immutable. By contrast, the microscopic theory could discover situations (materials) where this is not so. The same thing can be said about deviations of θ from $\pi/2$ as a function of z or, indeed, the xy dependence of both θ and ϕ.

(c) Of course, first-principles calculations not only yield $\vec{M}(\vec{r})$ but also the changes in the electronic structure due to the deviation of $\vec{M}(\vec{r})$ from its saturation value, namely the presence of a Bloch wall. In other words, they describe the electronic structure which supports, consistent with, a Bloch wall. This information becomes available in the calculations we shall report.

(d) The change in the electronic states due to the presence of a Bloch wall is, or can be viewed as a description of the electron–Bloch wall interaction. Clearly, a study of this interaction will make an important contribution to understanding the widely observed magneto-transport phenomena associated with electrons scattering off Bloch walls.[11–14]

(e) Inevitably, a magnetic inhomogeneity will distort the underlying lattice and such distortions give rise to Bloch wall-Bloch wall interactions and pinning of Bloch walls by lattice defects like impurities vacancies or grain boundaries.[1] Although we do not deal with the appropriate generalization of our first-principles approach, we wish to stress that it can be readily adopted to address these issues and this possibility is an important part of the motivation for perusing it.

Finally, we comment on our choice of bcc iron as the host to the Bloch wall in our calculations. As is well known the saturation magnetic moment per atom μ_{s} at $T=0$ and the effective moment μ_{eff} deduced from the Curie constants, measured at $T>T_{\mathrm{C}}$, for metallic ferromagnets are usually not the same. In fact, the deviation of $\mu_{\mathrm{s}}/\mu_{\mathrm{eff}}$ from 1 can be taken as a good measure of how independent the local magnetic moments are from their relative orientation. Since bcc iron is a famously good moment system, namely $\mu_{\mathrm{s}}\simeq\mu_{\mathrm{eff}}$, we expect the first-principles calculations to map optimally onto the phenomenological theory summarized by Eqs. (5) and (6). This is indeed what we find and we take this fact as a validation of our conceptual framework as well as our numerical procedures for implementing it. The prize to pay for having done this ''easy'' case is that the importance of all the features listed above (a)–(e) are minimized. Thus, if we disregard these interesting but small effects, our calculations reduce to a different, if complicated, way of computing the material dependent parameters, e.g., the spin-wave stiffness constant α and the anisotropy parameter β. As these are also available from other types of first-principles calculations,[15–18] the comparison of our results with those of others in the field is a useful exercise in its own right.

In the next section we shall describe the first-principles theoretical framework, based on a relativistic, spin-polarized density-functional theory, for our calculations. This is followed by a section describing the computational procedures. We shall present and discuss our results in Sec. IV, whereas in Sec. V. we shall evaluate the progress we have been able to make and the prospects of the microscopic approach we have advocated.

II. A FIRST-PRINCIPLES THEORY OF BLOCH WALLS

A fully relativistic density functional theory (DFT),[19,20] which includes the dipolar interaction between electrons, would, presumably, yield an inhomogeneous ground state with the domain structure determined by the size and shape of the sample. Clearly, the corresponding calculations are out of the question and we shall follow the logic of the phenomenological theory. Namely, we neglect the dipolar interaction and study a single Bloch wall engendered by the constraint that the magnetization $\vec{M}(\vec{r})$ is oriented along two different easy axes at $z\rightarrow\pm\infty$. This problem is readily encompassed by the spin-polarized relativistic density functional theory in the local density approximation (LDA) as usually applied in solid-state physics.[19,20] There are only two features of the way we shall proceed which deserve further general comment. Firstly, we note that we shall not be looking for a

ground state, as usual, but a lowest-energy state consistent with a constraint which prescribes a symmetry different from the ground state. Fortunately, as it is well known, DFT covers this eventuality.[19,20] Secondly, we shall not attempt to address the vexing conceptual difficulties that arise in connection with imposing constraints while solving self-consistently the Kohn-Sham-Dirac equation of the theory,[21] but in this preliminary exploration of the subject implement our strategy in the simplest possible way as outlined below.

There is no reason to doubt that the established phenomenological theory[9] in the introduction gets the essential physics of the Bloch wall formation right. From the point of view of formulating a first-principles version of this theory it may be summarized as follows: the changing orientation of $\vec{M}(z)$, namely the variation of $\phi(z)$ in Eq. (6), across the Bloch wall implies an exchange energy cost which is lower the slower the variation, whereas the anisotropy energy favors a rapid change from one easy direction, $\phi=0$, to the other, $\phi=\pi/2$, and the width of the transition region of $\phi(z)$ in Eq. (6), $l_{\mathrm{BW}}=\pi\sqrt{\alpha/\beta}$, is determined by the balance of these two tendencies. Indeed, we can bypass the solution of the Euler-Lagrange equation, which in the case of minimizing the free-energy $\mathcal{F}(\phi)$ in Eq. (5) is the famous Sine-Gordon equation whose solution is $\phi(z)$ in Eq. (6), and take $\phi(z)$ to be a simple function, $\phi_0(z/L)$, which goes from 0 to $\pi/2$ in a distance of L and minimize the corresponding free-energy $\mathcal{F}(L)$ with respect to the width L. As can be readily shown, by substituting $\phi_0(z/L)$ into Eq. (5), the free-energy per unit cell yields

$$\mathcal{F}(L)=\alpha I_1 A\frac{1}{L}+\beta I_2 AL, \tag{7}$$

where A is the area of the two-dimensional (2D) unit cell, and

$$I_1=\int \phi_0'(\xi)^2 d\xi \quad \text{and} \quad I_2=\int \sin^2\phi_0(\xi)\cos^2\phi_0(\xi)d\xi. \tag{8}$$

Clearly, the first term in Eq. (7), proportional to $1/L$, is due to the exchange interaction measured by α and the second term, which is proportional to L and the constant β, represents the contribution of the magneto-crystalline anisotropy energy for cubic systems. Furthermore, $\mathcal{F}(L)$ reaches its minimum at

$$L_{\min}\equiv l_{\mathrm{BW}}=\sqrt{\frac{\alpha I_1}{\beta I_2}}. \tag{9}$$

Given that I_1 and I_2 are simple dimensionless numbers which parametrize the profile $\phi_0(z/L)$, this result agrees well with the exact soliton solution for $I_1/I_2\simeq\pi^2$.

Evidently, the above discussion suggests a rather straightforward strategy for first-principles calculations: (a) assume a profile $\phi_0(z/L)$, (b) carry out a density functional calculation for the magnetization $\vec{M}(z)$ constrained to follow the profile $\phi_0(z/L)$ and calculate the total energy or grand potential $\Omega(L)$, (c) and minimize $\Omega(L)$ with respect to L.

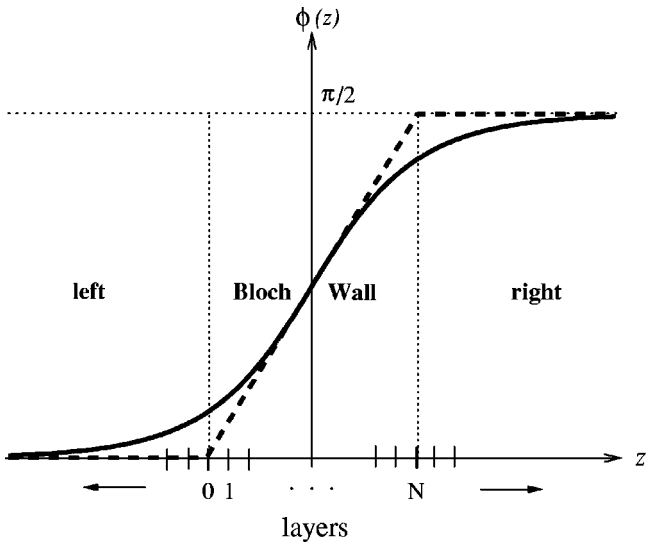

FIG. 2. Comparison of the soliton solution, Eq. (6), (solid line) and the linear magnetization profile, Eq. (10), (dashed line) used in our calculations. The numeration of the layers and the partitioning of the system into different regions as used in the actual calculations is also depicted on the picture.

For the profile we shall always take the particularly simple choice

$$\phi_0(\xi)=\begin{cases}0 & \xi<0\\ \xi\pi/2 & 0\leqslant\xi\leqslant 1,\\ \pi/2 & \xi\geqslant 1\end{cases} \tag{10}$$

which is compared to the soliton solution in Fig. 2. For this function $I_1=\pi^2/4$ and $I_2=1/8$ and hence if $\Omega(L)$ is given by Eq. (7)

$$\Omega(L)=\frac{A\pi^2}{4}\alpha\frac{1}{L}+\frac{A}{8}\beta L, \tag{11}$$

which implies $l_{\mathrm{BW}}=\sqrt{2}\pi\sqrt{\alpha/\beta}$. Note that this Bloch wall thickness is $\sqrt{2}$ times larger than that deduced from Eq. (6). Thus the Bloch wall thickness is to some extent an ill-defined concept in the present ''prescribed profile'' approach to the problem. As will be clear presently, our calculated $\Omega(L)$ can be fitted by the above functional form very accurately and hence it determines the coefficients α and β from first principles.

For orientation we note that via the Landau-Lifshitz equation, Eq. (1), the free-energy functional given in Eq. (5) implies a spin-wave dispersion relation. In the long wavelength limit this yields

$$\omega_q=\frac{4\beta\mu_{\mathrm{B}}}{M_0}+\frac{4\alpha\mu_{\mathrm{B}}}{M_0}q^2, \tag{12}$$

thus, the spin-wave stiffness constant

$$D=\frac{4\alpha\mu_{\mathrm{B}}}{M_0}, \tag{13}$$

and the usual cubic (fourth-order) anisotropy constant

$$K_4 = \frac{\beta a^3}{2}. \tag{14}$$

As expected, in the presence of magneto-crystalline anisotropy the spin-wave spectrum is gaped.

Without any account of dipolar interactions, in nonrelativistic quantum mechanics the orientation of the magnetization is independent from the crystal axis. As is clear from the above discussion, under this circumstance ($\beta=0$) there is no Bloch wall of finite width. Thus, our calculation of $\Omega(L)$ must include spin-orbit coupling which is the major source of magneto-crystalline anisotropy in transition metals.[22] Rather than treating the spin-orbit interaction in perturbation theory, we use a fully relativistic spin-polarized density functional theory.[19,20]

The natural variable in the microscopic theory is the magnetization averaged over a unit cell

$$\vec{m}_i = \int_{V_i} d^3 r \vec{m}(\vec{r}), \tag{15}$$

where V_i is the volume of the ith unit cell. We may then define the local orientation $\vec{e}_i$ by

$$\vec{e}_i = \vec{m}_i / m_i, \tag{16}$$

where m_i denotes the length of the vector $\vec{m}_i$. It is this effective local orientation that we wish to constrain to follow the discrete version of the profile in Eq. (10). Namely, we assume that $\vec{e}_p$ is the same within an atomic plane with position z_p and take

$$\vec{e}_p = \cos\phi_p \hat{x} + \sin\phi_p \hat{y}, \tag{17}$$

where for a 90° Bloch wall, which is N layer thick,

$$\phi_p = p\frac{\pi}{2N} \quad (p=1,\ldots,N). \tag{18}$$

Thus, we have to solve the Kohn-Sham-Dirac equation of DFT for the circumstance where the orientation of the magnetization, ϕ_p, is changing from layer to layer within a slab of N atomic layers and is uniformally 0 and $\pi/2$ to the left and right, respectively, of the slab as shown in Fig. 2. Evidently, the relativistic spin-polarized Screened-KKR method,[23] which treats just such geometries, is ideal for tackling this problem. Fortunately, the code which implements this method scales linearly with N and, as we shall demonstrate presently, can handle 800–1000 layers with readily available computer power.

III. THE COMPUTATIONAL METHOD

We performed calculations proposed in the previous section by using the spin-polarized relativistic screened Korringa-Kohn-Rostoker (SPR-SKKR) method.[23] Although the method is by now well-established (see also Refs. 24 and 25), for completeness and since we also made developments specific to the Bloch wall problem, we briefly outline our computational strategy. For an ensemble of individual scatterers the multiple scattering theory (MST) yields the one-electron Green function for an arbitrary complex energy z and real space coordinates $\vec{r}$, $\vec{r}\,'$

$$\begin{aligned}\mathcal{G}(z;\vec{r},\vec{r}\,') = &\sum_{QQ'} Z_Q^n(z,\vec{r}_n)\tau_{QQ'}^{nm}(z)Z_{Q'}^m(z,\vec{r}\,'_m)^\dagger \\ &- \delta_{nm}\sum_Q \{J_Q^n(z,\vec{r}_n)Z_Q^n(z,\vec{r}\,'_n)^\dagger\Theta(r_n - r'_n) \\ &+ Z_Q^n(z,\vec{r}_n)J_Q^n(z,\vec{r}\,'_n)^\dagger\Theta(r'_n - r_n)\},\end{aligned} \tag{19}$$

where n and m label two specific sites of position vectors $\vec{R}_n$ and $\vec{R}'_n$, while Q and Q' denote pairs of angular momentum quantum-numbers (κ,μ) and (κ',μ'), respectively. The functions $Z_Q^n(z,\vec{r}_n)$ and $J_Q^n(z,\vec{r}_n)$, regular and irregular at $\vec{r}_n \equiv \vec{r} - \vec{R}_n = 0$, respectively, are properly normalized solutions of the Kohn-Sham-Dirac equation related to a single, finite-ranged potential well for which we now assume a spherically symmetric effective potential, $V_n^{\rm eff}(r)$, and effective field, $B_n^{\rm eff}(r)$, pointing along a local (positive) z coordinate axis. In short,

$$\begin{aligned}&(c\vec{\alpha}\vec{p} + (\beta - I_4)mc^2 + I_4 V_n^{\rm eff}(r) + \beta\Sigma_z B_n^{\rm eff}(r) - zI_4) \\ &\times \begin{Bmatrix} Z_Q^n(z,\vec{r}) \\ J_Q^n(z,\vec{r}) \end{Bmatrix} = 0,\end{aligned} \tag{20}$$

where

$$\vec{\alpha} = \begin{pmatrix} 0 & \vec{\sigma} \\ \vec{\sigma} & 0 \end{pmatrix} \quad \beta = \begin{pmatrix} I_2 & 0 \\ 0 & -I_2 \end{pmatrix} \quad \Sigma_z = \begin{pmatrix} \sigma_z & 0 \\ 0 & \sigma_z \end{pmatrix}$$

$$I_4 = \begin{pmatrix} I_2 & 0 \\ 0 & I_2 \end{pmatrix}$$

with the usual Pauli matrices $\vec{\sigma}$ and the two-dimensional unity matrix I_2. The numerical solution of the above equation with a corresponding expression for the so-called single-site t matrix was originally given in Refs. 26 and 27. A particular feature resulting from the approach they used is that, although the t matrix has necessarily off-diagonal elements, no coupling between different l values is present.

We further simplify the problem by adopting the atomic sphere approximation (ASA) in which the volume of the sphere is taken equal to the volume of the corresponding Wigner-Seitz cell. Clearly, ASA deals with overlapping potentials which is, in strict sense, prohibited within the MST, however, mostly for inhomogeneous systems, this approach is widely used, since on one hand it gives a better description of the interstitial region than the muffin-tin approach, on the other hand it is conceptually much simpler than a full potential description. As implied above, our approach allows the orientation of the magnetization to vary from site to site as required in the case of a Bloch wall where we keep the orientation to be constant within the atomic planes but let it rotate from layer to layer around the global z direction.

Therefore, in each layer there will be a rotation R, corresponding to $\theta=\pi/2$ and $\phi=\phi_p$ [see Eq. (18)], which relates the t matrix in the local to that in the global coordinate system as follows

$$\underline{t}_{glob}(z)=\underline{\underline{D}}(R)\underline{t}_{loc}(z)\underline{\underline{D}}(R)^{\dagger}, \tag{21}$$

where $\underline{\underline{D}}(R)$ denotes a matrix containing, block wise, the irreducible representations of R.

As the solution of the above single-site problem is relatively easy and universal in applications of MST, the evaluation of the scattering path operator (SPO), $\tau^{nm}_{QQ'}(z)$ in Eq. (19), is, essentially, the main difficulty in such calculations. The geometrical arrangement of the scatterers involved in the system is put, in MST, into the so-called structure constants, $G^{nm}_{QQ'}(z)=G_{QQ'}(z;\vec{R}_n,\vec{R}_m)$ $(\underline{\underline{G}}^{nm}(z)=\{G^{nm}_{QQ'}(z)\})$, which for the relativistic case can be obtained by a transformation in terms of the Clebsh-Gordon coefficients from its nonrelativistic counterpart (see, e.g., Ref. 28). By defining the corresponding matrices having both site and angular momentum indices[28]

$$\mathbf{t}(z)=\{\underline{t}^{n}(z)\,\delta_{nm}\},\quad \mathbf{G}(z)=\{\underline{\underline{G}}^{nm}(z)\},\quad \boldsymbol{\tau}(z)=\{\underline{\tau}^{nm}(z)\},$$

the SPO is given by the following matrix inversion

$$\boldsymbol{\tau}(z)=[\mathbf{t}(z)^{-1}-\mathbf{G}(z)]^{-1}. \tag{22}$$

A particular problem arises from the fact that $\underline{\underline{G}}^{nm}(z)$ is long ranged, therefore, the inversion in Eq. (22) cannot be directly performed. For a system with three-dimensional periodicity the problem can be exactly handled by making use of the lattice Fourier-transformation, which splits Eq. (22) into the corresponding $\vec{k}$ projections which has to be solved in angular momentum space only. The Bloch wall problem we deal with exhibits, however, two-dimensional (2D) periodicity in the (x,y) plane, while in the z direction the translational symmetry is broken due to the variation of the orientation of the magnetization. Thus employing 2D lattice Fourier-transforms

$$\underline{\underline{G}}^{pq}(z;\vec{k}_{\parallel})=\sum_{\vec{R}_{\parallel}} e^{\imath\vec{k}_{\parallel}\vec{R}_{\parallel}}\underline{\underline{G}}(z;\vec{C}_p+\vec{R}_{\parallel},\vec{C}_q), \tag{23}$$

where p and q denote atomic layers, generated by $\vec{C}_p$ and $\vec{C}_q$, respectively, $\vec{R}_{\parallel}$ are 2D lattice vectors and $\vec{k}_{\parallel}$ is a vector in the first 2D Brillouin-zone (BZ), and the new matrix notation in terms of layer indices

$$\mathbf{t}(z)=\{\underline{t}^{p}(z)\,\delta_{pq}\},\quad \mathbf{G}(z;\vec{k}_{\parallel})=\{\underline{\underline{G}}^{pq}(z;\vec{k}_{\parallel})\},$$

$$\boldsymbol{\tau}(z;\vec{k}_{\parallel})=\{\underline{\tau}^{pq}(z;\vec{k}_{\parallel})\},$$

one can write

$$\boldsymbol{\tau}(z;\vec{k}_{\parallel})=(\mathbf{t}(z)^{-1}-\mathbf{G}(z;\vec{k}_{\parallel}))^{-1}. \tag{24}$$

Evaluating the matrix inversion in Eq. (24) is still demanding since the structure constants involved are long ranged as far as the interlayer distances are concerned. In order to render this problem tractable the concept of ''screening'' has been introduced in the middle of the nineties.[25] Without going into details, a canonical transformation of the t matrices and the structure constants, which leaves the Green function invariant, in terms of repulsive scattering potentials makes it possible to reduce the spatial range of the effective structure constants. As this transformation is independent of the real scatterers in the system, it is very useful to perform self-consistent calculations, since it has to be performed for the structure constants only once at the beginning of calculation. In terms of the ''screened'' quantities Eq. (24) has exactly the same form. However, since $G^{pq}(z;\vec{k}_{\parallel})$ is now well localized, it can be truncated for $|p-q|>n$ at a given n ($\simeq 3$ for fcc and bcc principal facets), which in turn implies a block-tridiagonal form for the matrix $\mathbf{G}(z;\vec{k}_{\parallel})$. This blocks are related to the so-called ''principal layers'' containing n subsequent atomic layers. By splitting our system into left and right perfect semi-infinite subsystems, in each of them the scatterers are all identical (bulk), and into a central region, where the potentials as well as the orientation of the magnetization can vary, the projection of the SPO, Eq. (24), onto the central region can be calculated *exactly*, i.e., taking into account all the scattering events to the left and right semi-infinite regions.[24] A remarkable feature of the method is that, if only the layer diagonal blocks of the SPO need to be calculated, it scales linearly with the size of the central region, namely N.[29] Thus it opens the way for investigating systems with inhomogeneities extending much beyond the atomic scales such as Bloch walls.

Let us now turn to the task of performing the Brillouin-zone integration

$$\underline{\tau}^{nm}(z)=\int_{\Omega_{BZ}} d^2k_{\parallel}e^{-\imath\vec{k}_{\parallel}(\vec{R}_{\parallel}-\vec{R}'_{\parallel})}\underline{\tau}^{pq}(z,\vec{k}_{\parallel}), \tag{25}$$

where $\vec{R}_n=\vec{C}_p+\vec{R}_{\parallel}$ and $\vec{R}_m=\vec{C}_q+\vec{R}'_{\parallel}$, while Ω_{BZ} denotes the volume of the 2D BZ. In Ref. 23 we described a method for reducing the demand of the above BZ integration using the symmetry operations of the underlying lattice. This is obviously useless for the present case of the 90° Bloch wall, since the direction of the magnetization rotates from layer to layer, say, from the x axis to the y axis, therefore the Bloch wall itself is not invariant under any of the symmetry operations of the C_{4v} group characteristic to the BCC(001) BZ.

However, it is still useful to note that the magnetization direction described by the angle $\phi(z)$ in a 90° Bloch wall perpendicular to the (001) direction of a BCC lattice and satisfying the boundary conditions $\phi(-\infty)=0$ and $\phi(\infty)=\pi/2$ has the symmetry property

$$\phi(z)-\frac{\pi}{4}=-\phi(-z)+\frac{\pi}{4}. \tag{26}$$

Taking into account also the symmetry of the underlying lattice this implies that the Bloch wall is invariant under a 180^{o} rotation around the axis (110) which is in three dimensional space represented by the matrix

$$S_{\mathrm{BW}}=\begin{pmatrix} 0 & 1 & 0 \\ 1 & 0 & 0 \\ 0 & 0 & -1 \end{pmatrix}, \tag{27}$$

whereby the axis of the rotation should cross the z axis at $z=0$, i.e., for which $\phi(0)=\pi/4$. Quite clearly, $S_{\mathrm{BW}}^{-1}=S_{\mathrm{BW}}$. Also evidently, the 2D square BZ is invariant under S_{BW}.

To make use of this symmetry, let $\underline{U}$ be the unitary matrix which represents S_{BW} in the (κ,μ) space and p' denote the layer onto which a particular layer p is mapped by S_{BW}. Then for the corresponding single-site t matrices we can write

$$\underline{t}^{p'}(z)=\underline{U}\underline{t}^{p}(z)\underline{U}^{\dagger}. \tag{28}$$

By introducing

$$\mathbf{U}=\{\underline{U}_{pq}\}, \quad \underline{U}_{pq}\equiv\underline{U}\delta_{qp'}, \tag{29}$$

or alternatively, by taking the choice of $p'=-p$,

$$\mathbf{U}=\begin{pmatrix} & 0 & 0 & \underline{U} & \\ \ldots & 0 & \underline{U} & 0 & \ldots \\ & \underline{U} & 0 & 0 & \end{pmatrix} \tag{30}$$

it follows that

$$\mathbf{t}(z)=\mathbf{U}\mathbf{t}(z)\mathbf{U}^{\dagger}. \tag{31}$$

A relationship between the 2D Fourier-transformed structure constants with arguments $\vec{k}_{\parallel}$ and $\vec{k}'_{\parallel}=S_{\mathrm{BW}}\vec{k}_{\parallel}$ can also be established using the transformation of the real-space structure constants

$$\underline{G}(z;S_{\mathrm{BW}}\vec{R},S_{\mathrm{BW}}\vec{R}')=\underline{U}\underline{G}(z;\vec{R},\vec{R}')\underline{U}^{\dagger}. \tag{32}$$

Therefore, by using Eq. (23) we can proceed as follows

$$\begin{aligned}\underline{G}^{p'q'}(z;\vec{k}_{\parallel})&=\sum_{\vec{R}_{\parallel}} e^{\imath\vec{k}_{\parallel}\vec{R}_{\parallel}}\underline{U} \\ &\quad\times\underline{G}(z;\vec{C}_p+S_{\mathrm{BW}}(\vec{R}_{\parallel}-\vec{R}_{\parallel}^{p}+\vec{R}_{\parallel}^{q}),\vec{C}_q)\underline{U}^{\dagger} \\ &=\sum_{\vec{R}_{\parallel}} e^{\imath\vec{k}'_{\parallel}\vec{R}_{\parallel}}\underline{U}\underline{G}(z;\vec{C}_p+\vec{R}_{\parallel}-\vec{R}_{\parallel}^{p'}-\vec{R}_{\parallel}^{q'},\vec{C}_q)\underline{U}^{\dagger} \\ &=\sum_{\vec{R}_{\parallel}} e^{\imath\vec{k}'_{\parallel}(\vec{R}_{\parallel}+\vec{R}_{\parallel}^{p'}-\vec{R}_{\parallel}^{q'})}\underline{U}\underline{G}(z;\vec{C}_p+\vec{R}_{\parallel},\vec{C}_q)\underline{U}^{\dagger} \\ &=e^{\imath\vec{k}_{\parallel}\vec{R}_{\parallel}^{p}}\underline{U}\underline{G}^{pq}(z;\vec{k}'_{\parallel})\underline{U}^{\dagger}e^{-\imath\vec{k}_{\parallel}\vec{R}_{\parallel}^{q}},\end{aligned} \tag{33}$$

where we defined $\vec{R}_{\parallel}^{p}=S_{\mathrm{BW}}\vec{C}_p-\vec{C}_{p'}$ and $\vec{R}_{\parallel}^{p'}=S_{\mathrm{BW}}\vec{R}_{\parallel}^{p}$, both being 2D lattice vectors. Thus, similar to Eq. (29), introducing

$$\tilde{\mathbf{U}}(\vec{k}_{\parallel})=\{\underline{\tilde{U}}_{pq}(\vec{k}_{\parallel})\}, \quad \underline{\tilde{U}}_{pq}(\vec{k}_{\parallel})\equiv e^{\imath\vec{k}_{\parallel}\vec{R}_{\parallel}^{p}}\underline{U}\delta_{qp'}, \tag{34}$$

Eq. (33) can be written compactly

$$\mathbf{G}(z,\vec{k}_{\parallel})=\tilde{\mathbf{U}}(\vec{k}_{\parallel})\mathbf{G}(z,\vec{k}'_{\parallel})\tilde{\mathbf{U}}(\vec{k}_{\parallel})^{\dagger}. \tag{35}$$

Clearly, the matrix $\tilde{\mathbf{U}}(\vec{k}_{\parallel})$ can also be used instead of $\mathbf{U}$ in Eq. (31), which immediately implies the following transformation property for the SPO

$$\boldsymbol{\tau}(z,\vec{k}'_{\parallel})=\tilde{\mathbf{U}}(\vec{k}_{\parallel})^{\dagger}\boldsymbol{\tau}(z,\vec{k}_{\parallel})\tilde{\mathbf{U}}(\vec{k}_{\parallel}). \tag{36}$$

As the above relationship makes possible to calculate the SPO only in half of the BZ when performing the integration in Eq. (25), the computational time and memory storage request of the computer code can be reduced by a factor of two. Alternatively, in the actual calculations we have made use of the above symmetry of the Bloch wall by halving the computational demand of the inversion in Eq. (24), while keeping all the $\vec{k}_{\parallel}$ points in the BZ. Although, this latter procedure is almost equivalent to what has been described above, as it facilitates the tridiagonal shape of the corresponding matrix,[29] its use is rather limited to localized schemes whereas the former one can be regarded to be quite general for calculations in Bloch wall problems.

For our present purposes the one-electron Green function, Eq. (19), can be used to calculate several quantities of interest such as the electronic density of states (DOS)

$$n(z)=-\frac{1}{\pi}\mathrm{Im}\int d^3r\ \mathrm{Tr}[\mathcal{G}(z;\vec{r},\vec{r})] \quad (z=\varepsilon+\imath\delta), \tag{37}$$

where the energy ε is real, δ is a small imaginary part serving as parameter of Lorentzian broadening, and Tr denotes trace of a matrix in the four-dimensional Dirac-space, the charge density

$$\rho(\vec{r})=-\frac{1}{\pi}\mathrm{Im}\int_{\mathcal{C}}dz\ \mathrm{Tr}[\mathcal{G}(z;\vec{r},\vec{r})], \tag{38}$$

where $\mathcal{C}$ is a semicircle contour in the upper complex semiplane starting at the bottom of the valence band, ε_{B}, and ending at the Fermi energy, ε_{F}, and the spin-density

$$\vec{m}(\vec{r})=-\frac{1}{\pi}\mathrm{Im}\int_{\mathcal{C}}dz\ \mathrm{Tr}[\beta\vec{\Sigma}\mathcal{G}(z;\vec{r},\vec{r})]. \tag{39}$$

Furthermore, the charge, the spin-moment and the band energy can be obtained straightforwardly as

$$Q=\int_{\mathcal{C}}dz n(z)=\int d^3r\rho(\vec{r}), \tag{40}$$

$$\vec{m}=\int d^3r\vec{m}(\vec{r}), \tag{41}$$

and

$$E_{\mathrm{b}}=\int_{\varepsilon_{\mathrm{B}}}^{\varepsilon_{\mathrm{F}}}d\varepsilon\,\varepsilon n(\varepsilon)=-\frac{1}{\pi}\mathrm{Im}\int_{\mathcal{C}}dz z\int d^3r\ \mathrm{Tr}[\mathcal{G}(z;\vec{r},\vec{r})], \tag{42}$$

respectively. From Eq. (19) it is quite obvious that the above quantities can readily be resolved into components with respect to cells (layers) as we shall show them when we present are results in the forthcoming sections.

By solving the Poisson-equation for the electrostatic potential and employing spin-density functional theory in the local approximation[30] for the exchange-correlation potential and exchange field, self-consistent calculations can be performed. First we carried out self-consistent calculations for BCC bulk iron, where we have used a theoretical lattice constant of $a=5.204$ a.u. derived by recent careful full-potential calculations.[31] In that calculation we kept the orientation of magnetization along the (100) easy axis and used 91 k points in the irreducible wedge of the 2D BZ (IBZ) for the BZ integrations, Eq. (25). For the energy integrals, Eqs. (40) and (41) we used 16 points along the semicircle sampled according a Gaussian-quadrature, while the corresponding summations in angular momentum space were subject to a cut-off of $l_{\max}=2$. We converged the Fermi energy to get the corresponding charge ($Z=27$) to an accuracy of 10^{-8} electrons. Note, that in our present approach, because of the equilibrium with the left (and right) semi-infinite regions, this Fermi level has to be also used in the calculations of the (finite-size) Bloch wall.

As mentioned earlier, we have made use of different approximations to calculate the free energy. The first, computationally less demanding one is based on the frozen-potential approximation frequently used also in magneto-crystalline anisotropy calculations (see Ref. 23 and Refs. therein). Briefly, we used the self-consistent bulk potential and effective field magnitude in each layer of the Bloch wall and we set the orientation of the exchange field by rotating successively the bulk t matrix from layer to layer, Eq. (21), according to the prescribed function $\phi_0(z)$. In this case only one iteration, to calculate the single-particle (band) energy and the charges, were carried out. As the charge neutrality (number of particles) is not preserved for the fixed volume of the central region, the grand-canonical potential has to be considered. For any thickness N of the Bloch wall, taking always the difference with respect to the ferromagnetic state, this is approximated by

$$\Delta\Omega(N)=\Delta E_{\rm b}-\epsilon_{\rm F}\Delta Q=\sum_p\ (\Delta E_{{\rm b},p}-\epsilon_{\rm F}\Delta Q_p). \quad (43)$$

The other approach is a fully self-consistent one. Unfortunately, the computer power available to us was sufficient for only a few such calculations. Therefore, only for the case of $N=60$ shall we present and discuss the changes in the electronic structure and magnetic moments due to the Bloch wall.

IV. RESULTS

A. The frozen potential calculations of Bloch wall energies

We have calculated the Bloch wall formation energy $\Delta\Omega(N)$ for various values of N using the frozen potential approximation. Note, that the summation in Eq. (43) has to be, in principle, taken over all the layers in the system. Our calculations show that layers more than about ten layers away from the wall do not contribute significantly to the sum although ΔE_p and ΔQ_p by themselves differ considerably from zero even far away from the wall.

As well-known, in the phenomenological theory,[9] the exchange energy and the magneto-crystalline energy contribute equally to the Bloch wall energy. Experimentally, for bcc Fe the magneto-crystalline anisotropy constant, K_4, is found to be 0.3 μRyd per atom,[32] while careful (nonorbital-polarized) LDA calculations predict 0.1–0.2 μRyd (see Ref. 18 and Refs. therein and note that for a cubic system $K_4=3[E(111)-E(100)]$.) This, on one hand, implies, that the Bloch wall energy normalized to one layer is expected to be of the same order of magnitude as the anisotropy energy and, on the other, we have to calculate the Bloch wall energy to the same accuracy as is necessary in magneto-crystalline anisotropy calculations.

The main difficulty arises from the fact that, in particular, close to the real energy axis one has to sample a high number of $\vec{k}_\parallel$ points when performing the BZ integration in Eq. (25). To reduce this problem we smoothened the energy integrals in Eqs. (40) and (42) by the Fermi function at a finite temperature T, taking into account the poles of it below the contour $\mathcal{C}$. Both from an analysis of the integrand and by checking it numerically, it turns out that the contour can be deformed to infinity in the upper complex semiplane. Moreover, only a finite number of Matsubara poles, $z_j=\epsilon_{\rm F}+\imath(2j+1)\pi k_{\rm B}T$ ($j=0,1,2,\ldots$), has to be considered. Assuming a quadratic T dependence of $\Delta\Omega(N;T)$ due to the Sommerfeld expansion, in order to perform extrapolation to $T=0$ it was necessary to take two different T values only.

In our calculations we choose 300 K and 150 K for these two temperatures by using 32 and 40 Matsubara poles with 1275 and 2926$\vec{k}_\parallel$ points in the 2D IBZ for z_0 (6 and 3 mRyd), respectively. These values were shown to be sufficiently high to yield converged bulk anisotropy energies which we calculated to check the reliability of our numerical evaluations with respect to other methods and also to compare to the value that can be deduced from the Bloch wall energies [see Eq. (14)]. For $T=300$ K and 150 K we got $K_4=0.142$ and 0.154 μRyd, respectively, which were extrapolated to $K_4=0.158$ μRyd at $T=0$. Obviously, this is a very good agreement with the results of other first-principles calculations.

Let's now turn to the results for the Bloch wall energies, associated with an area of size a^2, where a is the lattice constant of our bcc lattice, as a function of thickness L, measured in units of a ($2L/a=N$), shown in Fig. 3 for $T=150$ K and $T=300$ K as diamonds and crosses, respectively. The first thing to note is that the calculated points are very well fitted by the expression Eq. (11) as drawn by solid and dashed lines, respectively. The resulting values for

$$\hat{\alpha}\equiv\frac{\alpha\pi^2 a}{4}\ \text{and}\ \hat{\beta}\equiv\frac{\beta a^3}{8}$$

are listed in Table I together what fitted for $T=0$.

The fitted curves have their minima at 424 and 401 lattice parameters for $T=300$ K and $T=150$ K, respectively. Note that there is a point on the $T=300$ K curve which is beyond the minimum and hence we can be said to have crossed the scale gap. The minima are very shallow due to the smallness

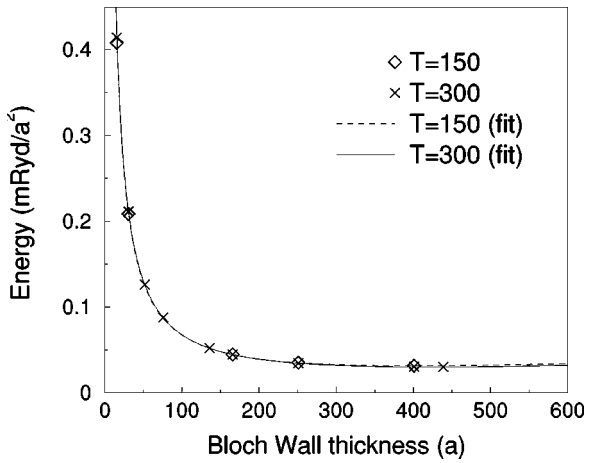

FIG. 3. Bloch wall energy as a function of the Bloch wall thickness. The diamonds and crosses stand for the results from the frozen potential calculations for $T=150$ K and $T=300$ K, respectively, with corresponding fits to the function Eq. (11) displayed in order by the dashed and solid lines.

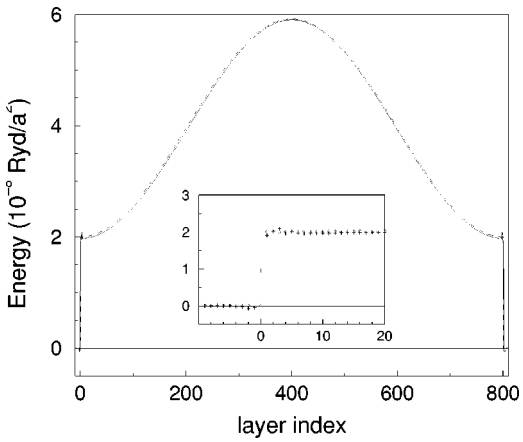

FIG. 4. Layer resolved energies for a 800 layer Bloch wall. The full line (crosses in the inset) show the result from the frozen potential calculation at $T=150$ K. The inset shows a magnification of the border area. The dashed line (diamonds in the inset) show the layer resolved energy contributions according to Eq. (44) of the phenomenological theory with parameters taken from Table I.

of the anisotropy energy, thus, this is likely to be a feature of calculations for all cubic systems.

From the extrapolated values of $\hat{\alpha}$ and $\hat{\beta}$ to $T=0$, $K_4=0.16$ μRyd, and $D=262$ meV Å^2 can be derived via Eqs. (13) and (14). By using the expression of l_{BW} from the phenomenological theory we also obtained a thickness of 394 lattice parameters for the Bloch wall. Several experimental values can be found for D, e.g., 314 meV Å^2 by Stringfellow,[33] 281 meV Å^2 by Collins *et al.*[34] or 280 meVÅ^2 by Mook and Nicklow.[35] So our value is only slightly below the experimental findings. The same is true for the comparison with other theoretical results found from bulk calculations.[15,16] One source of discrepancies between our and other calculations is certainly the use of different lattice constants. It is, however, worth noting that by using the same computer code and a spin-flip technique, in the scalar-relativistic limit, a value of $D=300$ meV Å^2 was calculated,[36] in better agreement with those calculated by others. This suggests that another source of the deviation of our present value from those of others arises from the relativistic approach we used, that is, the spin-orbit coupling gives not only rise to the magneto-crystalline anisotropy, but to some extent influences the spin-spin interaction parametrized by D.

The value of the anisotropy constant is of greater concern. As it is generally the case in LDA calculations,[17,18] the experimental value, 0.3 μRyd, is roughly a factor of two bigger than the theoretical results. However, the important point here is that we find the same value for K_4 as given above when we determine K_4 from bulk calculations demonstrating the internal consistency of our calculations.

TABLE I. Parameters derived from a least square fit of the data in Fig. 3 for $T=300$ K and 150 K to the function Eq. (11). In the last row the corresponding values from a quadratic interpolation to $T=0$ are found.

T [K]	$\hat{\alpha}$ [mRyd]	$\hat{\beta}$ [μRyd]
300	6.41	0.0356
150	6.32	0.0392
0	6.29	0.0404

As implied by Eq. (43) our calculation allows to resolve the Bloch wall formation energy into contributions related to layer. This than can be compared to the free-energy density of the Ginzburg-Landau theory.[9] Taking the mean value for each layer and in terms of the parameters introduced above, for a linear 90° Bloch wall this free-energy density reads

$$\epsilon_p=\begin{cases}\dfrac{2\hat{\alpha}}{N^2}+\hat{\beta}\sin^2(\phi_p) & \text{if } 1\leqslant p\leqslant N\\ 0 & \text{any way.}\end{cases} \tag{44}$$

In Fig. 4 the solid line and crosses in the inset display the layer-resolved contributions to the Bloch wall energy as calculated by our first-principles method for a 800 layer thick wall and $T=150$ K, while the dashed curve and the diamonds in the inset are evaluated by using Eq. (44) with the corresponding fitted parameters, $\hat{\alpha}$ and $\hat{\beta}$ (see Table I), that is no further fitting have been used. Apparently, the coincidence of the two curves is nearly perfect even in this ''atomic scale'' resolution of the Bloch wall energy. As is clear from Eq. (44), in the phenomenological theory the exchange contribution to the layer resolved energy is constant, which equals $2\hat{\alpha}/N^2$, inside the wall and zero outside. A characteristic deviation from that behavior is found for the first-principles values near the edge of the wall. The exchange contribution to the first layer outside the Bloch wall, i.e., to layers numbered by 0 and 801 in Fig. 4, is exactly half of the above constant value (see inset of Fig. 4). This is due to the nonlocal nature of the exchange couplings not accounted properly within the phenomenological theory. We note that Bloch wall formation can be discussed also by us-

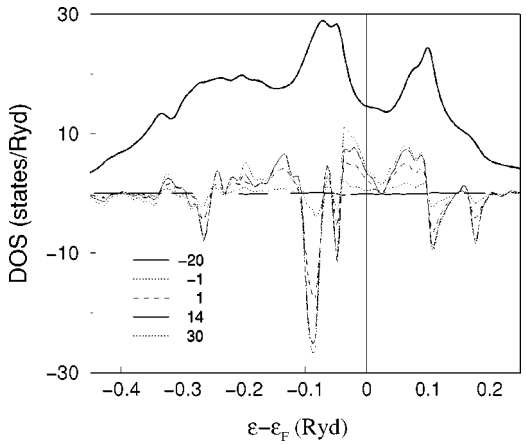

FIG. 5. The density of states (DOS) for bulk Fe bcc (thick line) together with their difference from the bulk for several layers in a 60 layer Bloch wall magnified by 1000. In the legend, negative/positive numbers label layers outside/inside the Bloch wall.

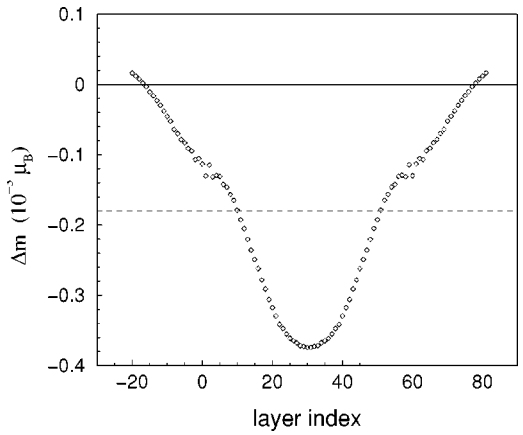

FIG. 6. The deviation of the magnetic moment from its value in the bulk, where it points in the easy direction (100), for each layer in a 60 layer Bloch wall. The dashed line indicates the moment obtained in a bulk calculation with the moment along the (110) direction.

ing an effective Heisenberg Hamiltonian with a cubic anisotropy term, in which the above feature is readily recovered. Small oscillations can also be seen near the edge of the Bloch wall. These are most likely related to Friedel-type oscillations, which in homogeneous systems arise due to any imperfections, as relaxations in the electronic structure.

B. Self-consistent calculation

In order to access reliably the electronic structure in the presence of a Bloch wall self-consistent calculations have to be performed. These calculations are not ground state calculations because the magnetic moment in every layer is forced to point along a prescribed direction. The proper way to perform such calculations is to introduce a constraining field which forces the moment to point along the chosen direction.[21] For our first attempts we ignored the constraining field and, instead, took the projection of the magnetic moment onto the prescribed direction after every iteration.

We have performed this calculation for a 60-layer Bloch wall with a magnetization profile according to Eq. (10). We allowed 21 layers on the two sides outside the Bloch wall to relax. That is, given the symmetry of the Bloch wall, 51 *different* potentials were involved in this calculation. The charging due to the Bloch wall per atom for the different layers works out to be smaller than $10^{-7}e$ and, therefore, can be considered to be zero within the accuracy of our calculations. This means we observed no charge redistribution (transfer) across the Bloch wall. Despite of this fact, as inferred from Fig. 5, the densities of states show characteristic changes for different layers in the Bloch wall. Interestingly, the biggest changes are found at energies also with big peaks in the bulk DOS, which presumably indicates lifting of some degeneracies, related to the cubic symmetry, due to the presence of Bloch wall.

Contrary to the charges, the magnetic moments display a small but clear deviation from their bulk value. In Fig. 6 we show the deviation of the moment from the bulk value. Obviously, the moments decrease gradually when approaching the center of the wall. Surprisingly, however, the moments outside the wall still quite differ from their bulk value, approaching it relatively far from the wall only. Similarly, at the center of the wall one would expect a moment equal to that calculated for a bulk with (110) hard axis. This value is shown by the dashed line in Fig. 6.

The component of the moment parallel to the wall but perpendicular to the exchange field is shown in Fig. 7. (One should note that the frame of reference is a local one which turns round with the exchange field.) Not surprisingly, the strong peaks appear at those layers which are just outside the Bloch wall, as these are the layers with the most asymmetric neighborhood. Clearly, these peaks are an artifact due to the prescribed magnetization profile which display pronounced kinks at the two borders of the Bloch wall (see Fig. 2). The component perpendicular to the wall is smaller than $10^{-5}\mu_B$ and therefore negligible.

These calculations were performed with 91 $\vec{k}_\parallel$ points in the two dimensional irreducible Brillouin zone. To achieve convergence roughly 100 iterations have been necessary

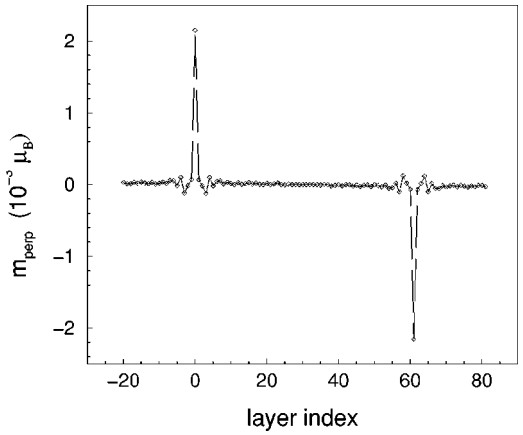

FIG. 7. The perpendicular component of the magnetic moment for each layer in a 60 layer Bloch wall.

(where one iteration took roughly 14 min on 16 nodes on a T3E). Clearly, the number of self-consistent iterations necessary to obtain reasonable convergence goes up with the number of layers and we have not been able to achieve convergence for thicker Bloch walls within the limited CPU time available to us. Due to the relatively small number of $\vec{k}_{\parallel}$ points used in this calculations we do not claim convergence for our results. But we expect the results to be qualitatively correct.

V. CONCLUSIONS

In short, we have presented a first-principles, that is to say parameter-free and yet materials specific, description of Bloch walls in ferromagnets. As an example we have prescribed the orientation of the magnetization density, $\vec{M}(\vec{r})$, to evolve from the easy axis (100) to (010) in BCC iron and calculated its energy, E_{BW}, as a function of the width, l_{BW}, of the transition region. To do this we used the fully relativistic spin-polarized density functional theory and solved the Kohn-Sham-Dirac equation by the SPR-SKKR method.[23] Due to the relativistic description of the electrons, their spin and orbital degrees of freedom were treated on equal footing and, hence, the calculation gave a full account of the magneto-crystalline anisotropy. Consequently, the Bloch wall energy had a minimum. The equilibrium width as well as the full curve, $E_{\mathrm{BW}}(l_{\mathrm{BW}})$ displayed in Fig. 3 was found to be in good agreement with available experimental data.

The novel feature of this kind of electronic theory of a Bloch wall, as compared to its conventional phenomenological description,[3] is that it provides an account of the distortions of the electronic structure due to the presence of the Bloch wall as well as its shape, width and energy. In particular, we have calculated the variations of the size of the magnetic moment, related to the local exchange splitting, and the local densities of states from layer to layer across the transition region. These results are displayed in Figs. 5 and 6. Evidently, these changes are small as expected on the grounds that bcc Fe is a good moment system. Nevertheless, even in this case they contain the essential information to describe the scattering of electrons by Bloch walls as one needs to do in a study of magneto-transport.[11–14]

Finally, we note that our calculations scale linearly with the number of layers, N, within the Bloch wall. Due to this fact we were able to perform calculations for up to 800 layers. That is to say we were able to describe a mesoscopic magnetic defect in fully first-principles terms.

ACKNOWLEDGMENTS

This work resulted from a collaboration partially funded by the TMR network (Contract No. EMRX-CT96-0089), the RTN Network ''Computational Magnetoelectronics'' (Contract No. RTN1-1999-00145), and the Hungarian National Science Foundation (Contract No. OTKA T030240 and T029813). One of us (J.S.) would like to thank the Computational Collaborative Project 9 of U.K. for financial support. Most of the computations were performed on the 3TE machine at the Manchester Computer Center of the EPSRC.

[1] A. Hubert and R. Schäfer, *Magnetic Domains* (Springer, Berlin, 1998).
[2] W. Heisenberg, Z. Phys. **69**, 287 (1931).
[3] F. Bloch, Z. Phys. **74**, 295 (1932).
[4] L. D. Landau and E. Lifshitz, Phys. Z. Sowjetunion **8**, 153 (1935).
[5] E. Lifshitz, J. Phys. (Moscow) **8**, 337 (1944).
[6] C. Kittel, Rev. Mod. Phys. **21**, 541 (1949).
[7] L. Néel, Comptes Rendus **241**, 533 (1955).
[8] W. F. Brown, *Micromagnetics* (Wiley, New York, 1963).
[9] A. M. Kosevich, in *Modern Problems in Condensed Matter Sciences, Vol. 17*, edited by V. M. Agranovich and A. A. Maradudin (North-Holland, Amsterdam, 1986), p. 495.
[10] B. A. Lilley, Philos. Mag. **41**, 792 (1950).
[11] T. Taniyama, I. Nakatani, T. Namikawa, and Y. Yamazaki, Phys. Rev. Lett. **82**, 2780 (1999).
[12] G. Tatara, Y.-W. Zhao, M. Muñoz, and N. García, Phys. Rev. Lett. **83**, 2030 (1999).
[13] J. B. A. N. van Hoof, K. M. Schep, P. J. Kelly, and G. E. W. Bauer, J. Magn. Magn. Mater. **177-181**, 188 (1998).
[14] J. B. A. N. van Hoof, K. M. Schep, and A. Brataas, Phys. Rev. B **59**, 138 (1999).
[15] A. I. Lichtenstein, M. I. Katsnelson, V. P. Antropov, and V. A. Gubanov, J. Magn. Magn. Mater. **67**, 65 (1987).
[16] H. Köhler, J. Sticht, and J. Kübler, Physica B **172**, 79 (1991).
[17] J. Trygg, B. Johansson, O. Eriksson, and J. M. Wills, Phys. Rev. Lett. **75**, 2871 (1995).
[18] S. S. A. Razee, J. B. Staunton, and F. J. Pinski, Phys. Rev. B **56**, 8082 (1997).
[19] R. M. Heizler and E. K. U. Gross, *Density Functional Theory* (Springer-Verlag, Berlin, 1990).
[20] P. Strange, *Relativistic Quantum Mechanics* (University Press, Cambridge, 1998).
[21] G. M. Stocks *et al.*, Philos. Mag. B **78**, 665 (1998).
[22] P. Bruno, in *Magnetismus von Festkörpern und Grenzflächen, 24. IFF-Ferienkurs* (KFA, Jülich, 1993), pp. 24.1.–28.
[23] L. Szunyogh, B. Újfalussy, and P. Weinberger, Phys. Rev. B **51**, 9552 (1995).
[24] L. Szunyogh, B. Újfalussy, P. Weinberger, and J. Kollár, Phys. Rev. B **49**, 2721 (1994).
[25] R. Zeller *et al.*, Phys. Rev. B **52**, 8807 (1995).
[26] R. Feder and F. Rosicky, Z. Phys. B: Condens. Matter **52**, 52 (1983).
[27] P. Strange, J. B. Staunton, and B. L. Györffy, J. Phys. C **17**, 3355 (1984).
[28] P. Weinberger, *Electron Scattering Theory for Ordered and Disordered Matter* (Clarendon, Oxford, 1990).
[29] E. M. Godfrin, J. Phys.: Condens. Matter **3**, 7843 (1991).
[30] S. H. Vosko, L. Wilk, and M. Nusair, Can. J. Phys. **58**, 1200 (1980).

[31] T. Korhonen, A. Settels, N. Papanikolaou, R. Zeller, and P. H. Dederichs, Phys. Rev. B **62**, 452 (2000).
[32] C. J. Tung, I. Said, and G. E. Everett, J. Appl. Phys. **53**, 2044 (1982).
[33] M. W. Stringfellow, J. Phys. C: Solid State Phys. **1**, 950 (1968).
[34] M. F. Collins *et al.*, Phys. Rev. **179**, 417 (1969).
[35] H. A. Mook and R. M. Nicklow, Phys. Rev. B **7**, 336 (1973).
[36] L. Udvardi and L. Szunyogh (unpublished).